Learnable antinoise-receiver algorithm based on a quantum feedforward neural network in optical quantum communication

Zhiguo Qu,[1,2,3,4,*] Xinzhu Liu,[2,†] and Le Sun[1,2,3]

[1]*Engineering Research Center of Digital Forensics, Ministry of Education, Nanjing University of Information Science and Technology, Nanjing 210044, China*

[2]*School of Computer Science, Nanjing University of Information Science and Technology, Nanjing 210044, China*

[3]*Jiangsu Collaborative Innovation Center of Atmospheric Environment and Equipment Technology, Nanjing University of Information Science and Technology, Nanjing 210044, China*

[4]*Information Security Center, State Key Laboratory of Networking and Switching Technology, Beijing University of Posts and Telecommunications, Beijing 100876, China*

(Received 23 November 2021; revised 17 April 2022; accepted 22 April 2022; published 19 May 2022)

The quantum communication process usually consists of three stages: the sender who prepares encoded carriers, the transmission in noisy channels, and the quantum receivers. The transmitted quantum information can be inevitably affected by kinds of quantum noise in the environment. Thus, quantum protocols are extensively studied to improve communication efficiency and accuracy under the influence of quantum noise. The optimization strategies usually occur in these three stages. In this paper, we focus on the optimization strategy of quantum receivers in the third stage. In quantum receiver algorithms, the key to distinguish received non-orthogonal coherent states in free-space optical quantum communication is to construct an optimum displacement operator for transforming the current coherent state into a state that is easier to distinguish than before. To improve the antinoise ability and accuracy of quantum communication, this paper proposes a universal optimization strategy of quantum receivers called learnable antinoise receiver (LAN receiver). In this strategy, a parametrized quantum circuit is constructed as a quantum feedforward neural network as the displacement operator to improve the antinoise ability. The parameters used in the quantum circuit are updated by gradient descent continuously to find the best parameter combination of the quantum circuit that minimizes the error rate and the qubits affected by quantum noise are used as training and testing data. The simulation of the proposed algorithm shows that the LAN receiver can resist different kinds of strong quantum noise. The average error rate of the proposed algorithm LAN receiver under the strong noise channel is 0.18, which has better performance than other type of receivers under the influence of strong quantum noise.

DOI: 10.1103/PhysRevA.105.052427

I. INTRODUCTION

The security of optical quantum communication is guaranteed by mature technologies such as quantum key distribution (QKD) [1,2], quantum identity authentication [3,4], quantum secure direct communication (QSDC) [5–8], etc. So that the optical quantum communication has been broad applied in fields of communication where the received light signal is extremely weak, such as satellite ground communication, deep space communication, and underwater communication. Among them, the communication techniques that encode all the information on qubits without sending classic bits are mainly studied in optical quantum communication.

With the development of optical photon quantum computers, the coherent state has been widely used as carrier to encode information due to its physical feasibility [9–13]. Therefore, a vital basic problem is how to distinguish nonorthogonal coherent states of encoded information under quantum noise effectively to ensure the security of quantum communication. However, it is well known that a quantum system in the real world cannot be a completely closed system since it will always interact with the outside world unavoidably. Such interactions are commonly referred to as quantum noise.

The study of optimizing quantum communications under the noisy environment has been carried out extensively. The quantum communication process usually consists of three stages: the sender who prepares encoded carriers, the transmission in noisy channels, and the quantum receivers. The optimization strategies usually occur in these three stages.

In the process of preparing encoded quantum carriers, the antinoise ability and communication accuracy can be improved by using optimized alphabets. For example, Dimario *et al.* [14] proposed an optimized alphabet in the first stage. It is proved to be robustness because the distinguishability does not get reduced under phase diffusion. Another commonly used method in this stage to survive photon losses in noise channels is encoding information into redundant quantum error-correcting codes. Lassen *et al.* [15] provide the experimental demonstration of the quantum erasure

*Corresponding author: qzghhh@126.com
†yzliubb@163.com

correcting code and investigated two approaches for circumventing inline losses. These approaches enhance the performance of long-distance quantum communication using quantum coherent states in noisy channels. During the process of the above-mentioned quantum communications, stable resources of squeezed light are in urgent need. Thus, Lassen *et al.* [16] also provides the experimental demonstration of quantum continuous variable measurements. In this work, the quantum averaging is implemented in linear system with feedforward.

In the process of transmission, the environment-assisted quantum erasing method is proposed to protect quantum information from being interfered with by noise environment. The environment can be measured in some way to recover quantum coherent states. It is also called the postselection procedure. The possibility of this method has been addressed by Filip and Andersen [17] and Gaussian noise is added in the decoherence process to simulate real environment. It is shown that this method has great potential to be employed into quantum key distribution schemes. The idea of quantum neural networks applies this postselection mechanism to a higher level that Mišta *et al.* proposed a method of minimal-disturbance measurement [18] which can be experimentally realized using a linear optics scheme with feedforward.

In the stage of receiving quantum information, displacement operation and the measurement operation are two main components of the quantum receivers. These operations help to improve distinguishability of nonorthogonal coherent states under the noisy environment. The early quantum receiver algorithms do not have strong antinoise ability. In the gradual development of quantum receivers, more and more researches focus on the improvement of antinoise ability.

Initially, Helstrom pioneered a closed-form solution to nonorthogonal coherent states discrimination for this problem [19]. The homodyne detection receiver is optimal when only Gaussian operation and classical communication are used and it provides a standard quantum limit (SQL) for the minimum error probability [20]. The best detector receivers that reach the Helstrom boundary have been proved feasible experimentally. However, these best detectors have a complex structure because they use real-time feedback techniques [21,22]. Therefore, it is of great practical significance to study the near-optimum technology with a simple implementation structure [23–27]. Kennedy proposed the first near-optimum receiver [23], which consists of a displacement operator and an on-off photodetector. When the average number of signal photons per classical bit is less than 0.4, the performance of the Kennedy receiver exceeds the classic homodyne detection receiver [20]. Afterwards, various improved receivers were widely proposed. For instance, two near-optimum receivers called Type-I receiver and Type-II receiver [20,28] were proposed representatively by Takeoka. These two receivers also consist of displacement operation and on-off photodetectors as the traditional Kennedy receiver. Receivers based on such experimental requirements are called generalized Kennedy receivers.

There is no doubt that the displacement operator in each receiver is indispensable because it improves the distinguishability of nonorthogonal coherent states. Take the encoded coherent states $|\pm\varphi\rangle$ used in the classic binary phase-shift keying communication protocol [13] as an example. The optimum displacement operator D is functioned on pure states $|\pm\varphi\rangle$ as

$$\begin{aligned} |\varphi\rangle &\xrightarrow{D(\xi)} |2\varphi\rangle, \\ |-\varphi\rangle &\xrightarrow{D(\xi)} |0\rangle. \end{aligned} \tag{1}$$

The quantum receivers with this type of displacement operator mentioned above are not robust enough when the system suffers from quantum noise [29–31]. Therefore, the capability to resist quantum noise has become more and more important for improving the performance of quantum receivers. A recently proposed conditional dynamics based (CD)-Kennedy receiver algorithm based on conditional dynamics [32] shows its capacity to resist noise. Its displacement operator is dynamically controlled by the input quantum state affected by quantum channel noise, meanwhile the threshold detection is introduced to improve the accuracy of the receiver. It is inspiring that setting the displacement operator as a dynamic operator conditioned by the input quantum state affected by noise can resist the influence of noise to some extent and be more robust in practical applications.

With the development of classical machine learning [33] in recent years, it has been considered to combine machine-learning technology with some widely used quantum algorithms. For example, Wallnöfer *et al.* [34] found that reinforcement learning has shown great potential in the field of quantum communication in a noisy environment due to its great power in the context of big-data analysis, classification, and prediction problems. They utilized reinforcement learning in the process of designing long-distance communication schemes. In this method, projective simulation is considered as the agent in the stochastic environment. It is proved that the learning agent can rediscover common quantum communication problems like teleportation and entanglement purification. Some quantum algorithms have shown the great advantage of quantum computing such as Fourier transform, Grover searching algorithm, quantum counting algorithm, and the Shor Algorithm. The combination of machine-learning methods and quantum computing algorithms will play a big role in quantum communication to process quantum information. The Harrow-Hassidim-Lloyd (HHL) algorithm [35] with phase estimation as the core and various HHL-like algorithms [36] proposed in 2009 greatly promoted the development of quantum machine learning. Subsequently, a series of quantum machine-learning algorithms emerged, such as the quantum support vector machine algorithm proposed in 2014 [37], the quantum principal component analysis algorithm [38], and the quantum generative adversarial network proposed in 2018 [39]. These algorithms vigorously promote the development of quantum machine learning. So far, one of important research branches of quantum machine learning is the quantum neural networks [40,41].

This paper proposes an optimization strategy called learnable antinoise receiver (LAN receiver) in which a quantum feedforward neural network is constructed as a displacement circuit which offers better performance under strong turbulent influence compared with traditional displacement operators. A parametrized quantum circuit is constructed to realize a

quantum feedforward neural network and the gradient descent method is used to update the parameters. Since the dynamic displacement based on the input qubits affected by quantum noise can be more robust to a certain extent, this algorithm uses the qubits affected by noise as the input data of the training data in order to improve the capacity of receiver on resisting quantum noise. This article analyzes the influence of quantum noise on the LAN receiver strictly and proves the antinoise performance of this receiver by simulations.

The content of this paper is arranged as follows: First of all, the preliminary knowledge related to this article is introduced in Sec. II. Second, the specific algorithm of LAN receiver based on quantum feedforward neural network and its corresponding practical physical realization are given in Sec. III. Then the performance analysis of the influence by quantum noise and the simulation on LAN receivers are performed in Sec. IV. At last, a summary of this article and the prospects for future research are described in Sec. V.

II. PRELIMINARY

An optical photon is an ideal physical realization of a quantum bit. Photons are neutral particles and do not have strong interactions with most matter. Photons can be transmitted in optical fibers over long distances with low loss. Physical devices such as mirrors, phase shifters, and beam splitters can be used to realize basic quantum operations in optical quantum computer. The noisy intermediate-scale quantum (NISQ) computer has shown the feasibility of the optical quantum computer [42].

A. Physical representation of qubits

Qubits can be represented by photons in the manner below in optimal quantum communication.

Consider two cavities with a total energy of $\hbar\omega$, and take two possible states of the qubit as being whether the photon is in the cavity ($|01\rangle$) or in another cavity ($|10\rangle$). The corresponding physical state of superposition is $c_0|01\rangle + c_1|10\rangle$ and this is called the dual-rail representation. The state of the photon in these two cavities corresponds to logical bits $|0_L\rangle$ and $|1_L\rangle$, which correspond to 0 and 1 classical bits in communications, respectively. By analogy, $2n$ $(n = 1, 2, \ldots)$ cavities can be used to represent logical qubits.

In the laboratory, the laser outputs a coherent state, which generates single photons. The coherent state in infinite-dimensional Hilbert space can be expressed as

$$|\alpha\rangle = \mathrm{e}^{-|\alpha|^2/2} \sum_{n=0}^{\infty} \frac{\alpha^n}{\sqrt{n!}} |n\rangle. \tag{2}$$

Here, $|n\rangle$ is the energy eigenstate of n photons. The mean energy of the coherent state is $\langle\alpha|n|\alpha\rangle = |\alpha|^2$. A coherent state is an eigenstate of the photon annihilation operator so that coherent state has a wide range of applications in optical quantum communication.

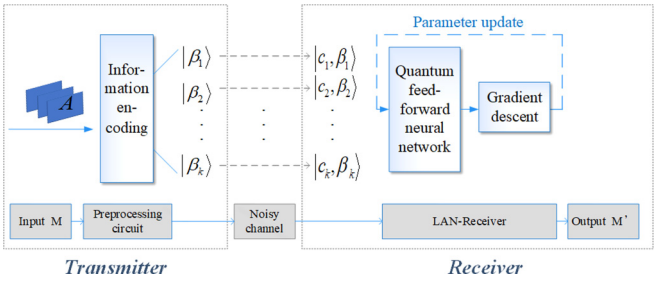

FIG. 1. LAN-receiver-based quantum communication system.

B. Devices for manipulating photon states

Three of the most experimentally accessible devices for manipulating the state of photons are the phase shifters, beam splitters, and cavity quantum electrodynamic systems.

(1) A phase shifter P is a slab of a transparent medium with a refractive index n different from that of free space n_0. In such a medium, the propagation distance is L with the phase of the photon changes to e^{ikL} where $k = \frac{n\omega}{c_0}$ and c_0 is the speed of light in vacuum. The corresponding Hamiltonian is

$$H = (n_0 - n)Z. \tag{3}$$

The operation of phase shifter is given by

$$P = \exp\left\{-\frac{iHL}{2c_0}\right\} = \exp\left\{-\frac{i\Delta Z}{2}\right\}. \tag{4}$$

The action of P on the coherent state $|\alpha\rangle$ is given by

$$P|\alpha\rangle = |e^{i\Delta}\alpha\rangle. \tag{5}$$

(2) A beam splitter B is a partially-silver-plated glass that reflects the fraction R of the incident light and transmits $1 - R$. Its function is to couple two coherent beams. The angle θ of the beam splitter is defined as $\cos\theta = R$. The relationship between inputs and outputs of the beam splitter is

$$a_{\mathrm{out}} = a_{\mathrm{in}} \cos\theta + b_{\mathrm{in}} \sin\theta, \tag{6}$$

$$b_{\mathrm{out}} = -a_{\mathrm{in}} \sin\theta + b_{\mathrm{in}} \cos\theta. \tag{7}$$

Note that unitary operations of any single qubit can be realized by using beam splitters and phase shifters.

(3) An optical cavity quantum electrodynamic system S solves the problem that the Kerr medium is difficult to find in the laboratory in traditional nonlinear optics. The C-QED system S consists of a Fabry-Perot cavity containing some atoms coupled to the optical field. The cavity is composed by two partially-silver-plated mirrors.

III. OPTICAL QUANTUM COMMUNICATION BASED ON LEARNABLE ANTINOISE RECEIVER

A. The optical quantum communication system

The configuration of quantum communication system with learnable antinoise receiver is shown in Fig. 1. The system consists of three stages: the sender with encoded carriers, the noisy channels, and our optimized quantum receiver. Usually, the optimization can be carried out in these three stages. In our algorithm, we mainly optimize the displacement operator of quantum receiver in the third stage. This is a universal method

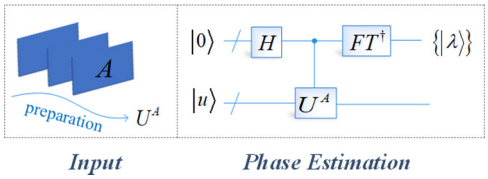

FIG. 2. Preprocessing circuit (a): conversion of the format of input classical data and feature extraction.

that other quantum communication schemes can also be optimized in the third stage using this proposed optimization quantum receiver.

To improve the efficiency and accuracy of the LAN receiver, it is reasonable to preprocess the input big data. So, the first step is to preprocess input data M by extracting features from it while encoding M into coherent states $\{|\beta_i\rangle,\ i = 1, 2, \ldots, k\}$. Then, transmit encoded pure states $\{|\beta_i\rangle,\ i = 1, 2, \ldots, k\}$ to a LAN receiver through the noisy channel. Next, the LAN receiver receives entangled quantum states $\{|c_i, \beta_i\rangle,\ i = 1, 2, \ldots, k\}$ and processes them by a quantum feedforward neural network to obtain the ideal output M'.

B. Optical quantum communication scheme based on the learnable antinoise receiver

1. Data preprocessing

Step 1 Convert format of input data. Transform different types of input data such as text, picture, audio, and so on into the form of the matrix and then transform it into the unitary matrix A.

Step 2 Extract feature from input data. Perform feature extraction on A by executing phase estimation. The eigenvalues of A can be obtained as $\{|\lambda\rangle^i = |\lambda_1 \ldots \lambda_d\rangle^i,\ i = 1, 2, \ldots, k\}$.

In Fig. 2, the premise of phase estimation is the effective simulation of A while A may be a nonsparse matrix which is not easy to simulate. Therefore, we introduce the method of constructing a sparse unitary matrix approximately in Ref. [43] to turn A into a sparse unitary S_A.

Embed the elements of A into S_A according to

$$S_A = \sum_{j,k=1}^{N} A_{jk}|k\rangle\langle j| \otimes |j\rangle\langle k| \in \mathbb{C}^{N^2\times N^2}. \tag{8}$$

Each column of S_A contains an element of A. As is shown in Eq. (9), the exponentiation operation of A is realized by exponentiation and partial trace operation of to approximately construct the unitary matrix:

$$\begin{aligned} tr_1\{e^{-iS_A\Delta t}\rho \otimes \sigma e^{iS_A\Delta t}\} &= \sigma - i\frac{\Delta t}{N}[A, \sigma] + O(\Delta t^2) \\ &\approx e^{-i\frac{A}{N}\Delta t}\sigma e^{i\frac{A}{N}\Delta t}. \end{aligned} \tag{9}$$

Here, σ is correspond to the target state of the power of the matrix $\frac{A}{N}$. The multiple copies of the density operator ρ are functioned as auxiliary quantum states. In Step2, the input data will be preprocessed as shown in Fig. 2. The output states of the phase estimation circuit $\{|\lambda\rangle^i = |\lambda_1 \ldots \lambda_d\rangle^i,\ i = 1, 2, \ldots, k\}$ represents the feature of input data.

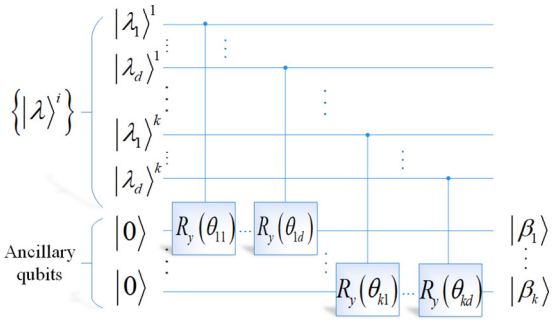

FIG. 3. Preprocessing circuit (b): feature encoding circuit where $\theta_{mn} > \theta_{mn+1}$ and $\theta_{mn} \in [0, \pi]$.

Step 3 Feature coding. Construct the circuit preprocessing circuit (b) in Fig. 3 to compress the k features obtained in Step 2 into k auxiliary qubits.

Step 4 The preprocessed data $\{|\beta_i\rangle,\ i = 1, 2, \ldots, k\}$ is transmitted to the receiver through the noisy channel and the receiver obtains the entangled states $\{|c_i, \beta_i\rangle,\ i = 1, 2, \ldots, k\}$. Then the LAN receiver is used to distinguish the transmitted non-orthogonal coherent states.

2. Learnable antinoise receiver

The learnable antinoise receiver is composed of a quantum feedforward neural network based on a parametrized quantum circuit. The key of realizing a quantum neural network is to find a model as a realization of linear and nonlinear functions.

The quantum neural network constructed in this paper is shown as Fig. 4, and its linear model is composed of parametrized unitary operators. Since the combination of phase gates and X, Y revolving gates can be used to realize arbitrary unitary operations on single qubit as

$$C_j^l = e^{i\tau}R_z(\varsigma)R_y(\xi)R_z(\zeta). \tag{10}$$

The construction of single-qubit controlled unitary gates is shown in Fig. 5. The single-qubit controlled unitary gates are functioned equivalent to a two-particle universal unitary gate.

The nonlinear model is composed of non-trace-preserving quantum operations. The non-trace-preserving quantum operations satisfy the relationship that $\sum_i E_i^\dagger E_i < I$. The extra information that appears during such quantum operations is obtained through measurement.

The parameters in the circuit are constantly updated and iterated during the process of training. When the value of

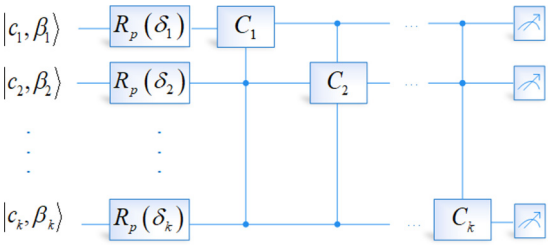

FIG. 4. Quantum neural network circuit for training displacement. Here, $p \in \{x, y, z\}$ and $\{\delta_i,\ i = 1 \ldots k\}$ denotes the rotation angle of the corresponding rotation operation $R_p(\delta_i)$.

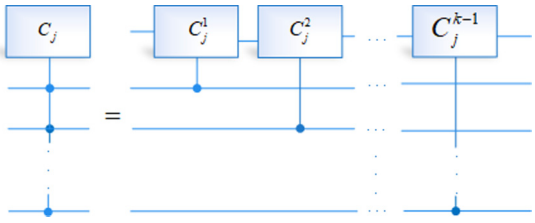

FIG. 5. Detailed description of the multiparticle-controlled circuit.

loss function in Eq. (11) reaches an ideal threshold, the parametrized quantum circuit becomes the optimal displacement circuit. The circuit of this quantum feedforward neural network is shown as Fig. 4. Figure 5 further presents the detailed description on the multiparticle-controlled circuit of C_j in Fig. 4.

As is shown in Fig. 4, the data set $\{(|\phi^i\rangle, y^i)|i = 1, \ldots, N\}$ is given. In the data set, $|\phi^i\rangle$ is the training data and $y^i \in \{0, 1\}$ is the corresponding category label. The mean square error function is used as the loss function:

$$\ell = \frac{1}{2N}\sum_{i=1}^{N}[y^i - f_{\{\delta,\tau,\varsigma,\xi,\zeta\}}(|\phi^i\rangle)]^2. \tag{11}$$

The initial values of the parameters of all unitary operators denoted as κ are randomly selected in $[0, 2\pi]$, and the gradient descent method is used for updating parameters. The gradient can be calculated as

$$\frac{\partial \ell}{\partial \kappa} = \frac{1}{2\varepsilon}[\ell(\kappa + \varepsilon) - \ell(\kappa - \varepsilon)] + O(\varepsilon^2). \tag{12}$$

At each iteration, the parameters are updated as

$$\kappa' = \kappa - \mu\frac{\partial \ell}{\partial \kappa}. \tag{13}$$

Here, μ is the learning rate and can be adjusted according to the convergence of the loss function. The output of the LAN receiver based on quantum neural network is denoted as M'.

C. A practical realization of LAN receiver

For the proposed parametrized quantum circuit of quantum neural network in LAN receiver, the corresponding components introduced in Sec. II can be used for physical realization.

The physical realization of the basic unitary operation is shown in Fig. 6. It can be seen from Sec. II that P represents a phase shifter which applies phase shift to a qubit. B represents a beam splitter, which couples two coherent beams. The cooperation of phase shifter and beam splitter helps to realize unitary operations. S represents the optical cavity quantum electrodynamics system that helps to realize nonlinear operations, such as the nonlinear coupling operation of qubits. The physical realization of the integral parametrized quantum circuit is shown as Fig. 7.

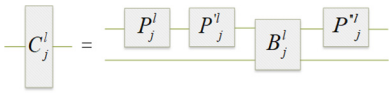

FIG. 6. The basic module of quantum neural network: the physical realization of arbitrary unitary operations

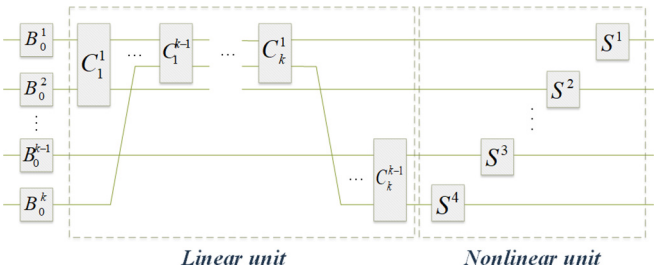

FIG. 7. Physical realization of quantum neural network circuit.

IV. FIDELITY ANALYSIS AND SIMULATION OF ANTINOISE PERFORMANCE

It is necessary to analyze the influence of quantum noise on quantum states because it inevitably exists in the process of quantum secure communication. It will interfere with the transmitted quantum states unavoidably and make the encoded information more difficult to identify. If the noise operators act on density operator $\rho \to \varepsilon(\rho)$, the quantum state will change from pure state into mixed state with information entropy increasing. According to the theorem whereby trace-preserving quantum operations are contractive; that is, for a trace-preserving quantum operation ε and density operators ρ and σ, the theorem is satisfied by

$$D(\varepsilon(\rho), \varepsilon(\sigma)) \leqslant D(\rho, \sigma). \tag{14}$$

That is, the physical process ε will shorten the trace distance between the two quantum states, which makes it more difficult to distinguish between the two quantum states.

In some cases, the real environment noise is simply simulated by Gaussian noise because the real noise is usually the combination of random noise with different probability distributions. However, the environment noise must be diversified in the real communication. Therefore, in the following content of this section, we analyze the influence of four kinds of common quantum noise: bit-flip, phase-flip, amplitude damping, and depolarizing noise, and their six combinations on quantum states in quantum secure communication.

A. Four kinds of quantum noise

There are four kinds of noise that usually affect on single qubit: bit flip, phase flip, amplitude damping, and depolarizing.

(1) Bit-flip noise

Similar to the bit flip of classical information, the bit-flip noise changes the state of a qubit from $|0\rangle$ to $|1\rangle$ or from $|1\rangle$ to $|0\rangle$ with a probability of $1 - \gamma$ and maintains the state of a qubit with a probability of γ. Its Kraus operators are

$$E_0 = \sqrt{\gamma}I, \quad E_1 = \sqrt{1-\gamma}X. \tag{15}$$

Here, I is the identity matrix, σ_x, σ_y, σ_z are the Pauli matrices, and γ is the noise parameter satisfying $0 \leqslant \gamma \leqslant 1$.

(2) Phase-flip noise

The phase-flip noise is defined as applying phase -1 to quantum state $|1\rangle$ with a probability of $1 - \gamma$ and maintains the state of a qubit with a probability of γ. Its Kraus operators

are

$$E_0 = \sqrt{\gamma} I, \quad E_1 = \sqrt{1-\gamma} Z. \tag{16}$$

(3) Amplitude damping noise

The amplitude damping noise describes the energy consumption under the effect of the quantum noise. The energy in quantum system will be lost to the environment due to the amplitude damping noise. Its Kraus operators are

$$E_0 = \begin{pmatrix} 1 & 0 \\ 0 & \sqrt{1-\gamma} \end{pmatrix}, \quad E_1 = \begin{pmatrix} 0 & \sqrt{\gamma} \\ 0 & 0 \end{pmatrix}. \tag{17}$$

Here, $\gamma = \sin^2(\theta)$ represents the probability of losing a photon.

(4) Depolarizing noise

Depolarizing noise is non-energy-dissipative noise. It depolarizes a qubit with a probability of $1-\gamma$ and maintains the state of a qubit with a probability of γ. Its Kraus operators are

$$E_0 = \sqrt{\gamma} I, \quad E_1 = \sqrt{\frac{1-\gamma}{3}} \sigma_X,$$
$$E_2 = \sqrt{\frac{1-\gamma}{3}} \sigma_Z, \quad E_3 = \sqrt{\frac{1-\gamma}{3}} \sigma_Y. \tag{18}$$

Two common measures of the distance between two quantum states ρ and σ are trace distance and fidelity. They are respectively defined as

$$D(\rho, \sigma) \equiv \tfrac{1}{2} \mathrm{tr}|\rho - \sigma|, \tag{19}$$

$$F(\rho, \sigma) \equiv \mathrm{tr}\sqrt{\rho^{1/2} \sigma \rho^{1/2}}. \tag{20}$$

The trace distance and fidelity are a pair of "reversed" concepts. The larger the trace distance between two states is, the smaller is the corresponding fidelity. The measurement used in the following analysis is fidelity.

Take $\alpha = \sqrt{0.1}$ for the coherent state given in Eq. (1), the corresponding superposition state is

$$|\alpha\rangle = \sqrt{0.90}|0\rangle + \sqrt{0.09}|1\rangle + \cdots. \tag{21}$$

For a coherent state in Eq. (21), if the light can pass through the attenuator successfully, it can be known, with a probability higher than 95%, that it is a single photon. And 90% of the time, it is the vacuum state that no photon will come through in cavity.

To analyze the influence of quantum noise in the channel on qubits in LAN receiver, the related analysis of fidelity and simulation of this algorithm using Python package TENSORFLOW QUANTUM are given below. Since the simulation platform is an ideal environment without noise, this paper superimposes quantum channel noise into the training and testing data of LAN receiver to illustrate the ability of the algorithm to resist quantum noise.

B. Fidelity analysis and simulation under different kinds of quantum noise

We analyze the corresponding fidelities of the noise affected system theoretically and superimpose the single noise or mixed noise into coherent state $\{|\beta_i\rangle,\ i = 1, 2, \ldots, k\}$ to get $\{|c_i, \beta_i\rangle,\ i = 1, 2, \ldots, k\}$ as the input of LAN receiver for simulation.

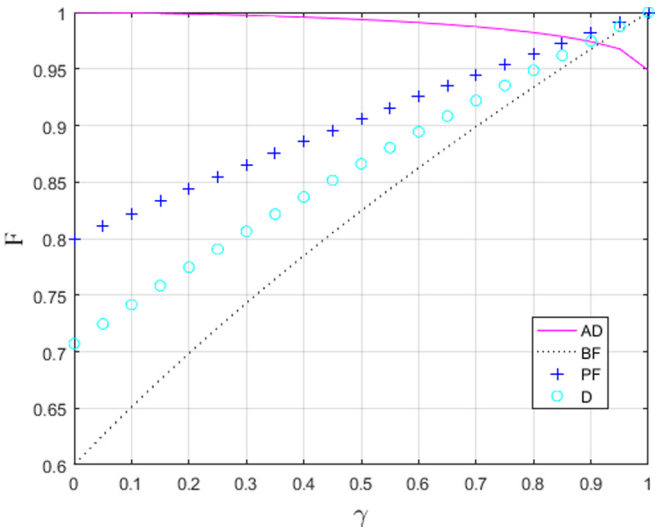

FIG. 8. Fidelity comparison under four kinds of single noise, amplitude damping (AD), bit flip (BF), phase flip (PF), and depolarizing (D).

1. Single noise

The corresponding fidelities are calculated as shown in Eqs. (22)–(25) respectively.

(1) Amplitude damping noise

$$F_{AD}(|\beta_i\rangle, |c_i, \beta_i\rangle) = (0.01\gamma^2 + 0.07\gamma + 0.18\sqrt{1-\gamma} + 0.82)^{1/2}. \tag{22}$$

(2) Bit-flip noise

$$F_{BF}(|\beta_i\rangle, |c_i, \beta_i\rangle) = (0.64\gamma + 0.36)^{1/2}. \tag{23}$$

(3) Phase-flip noise

$$F_{PF}(|\beta_i\rangle, |c_i, \beta_i\rangle) = (0.36\gamma + 0.64)^{1/2}. \tag{24}$$

(4) Depolarizing noise

$$F_D(|\beta_i\rangle, |c_i, \beta_i\rangle) = (0.5 + 0.5\gamma)^{1/2}. \tag{25}$$

Comparison of the fidelities under four different quantum noise is shown as Fig. 8.

It can be observed from Fig. 8 that the amplitude damping noise has the least impact on the communication system and the fidelity under the influence of amplitude damping noise is no less than 0.95. Bit-flip noise has the greatest impact on the system and the fidelity is reduced to the lowest value of 0.6. Note that the effect of the noise factor γ represents the probability of missing photons of amplitude damping noise, while the noise factor γ of the other three noise represents the probability that the quantum state remains unchanged. That is why the downward direction of the amplitude damping noise curve is different from that of the other three noise. For the amplitude damping noise, the greater the probability of losing photons, the greater the noise factor γ, the lower the fidelity. The fidelities of the quantum system under the influence of the remaining three noise decrease with the reduce of γ. Among

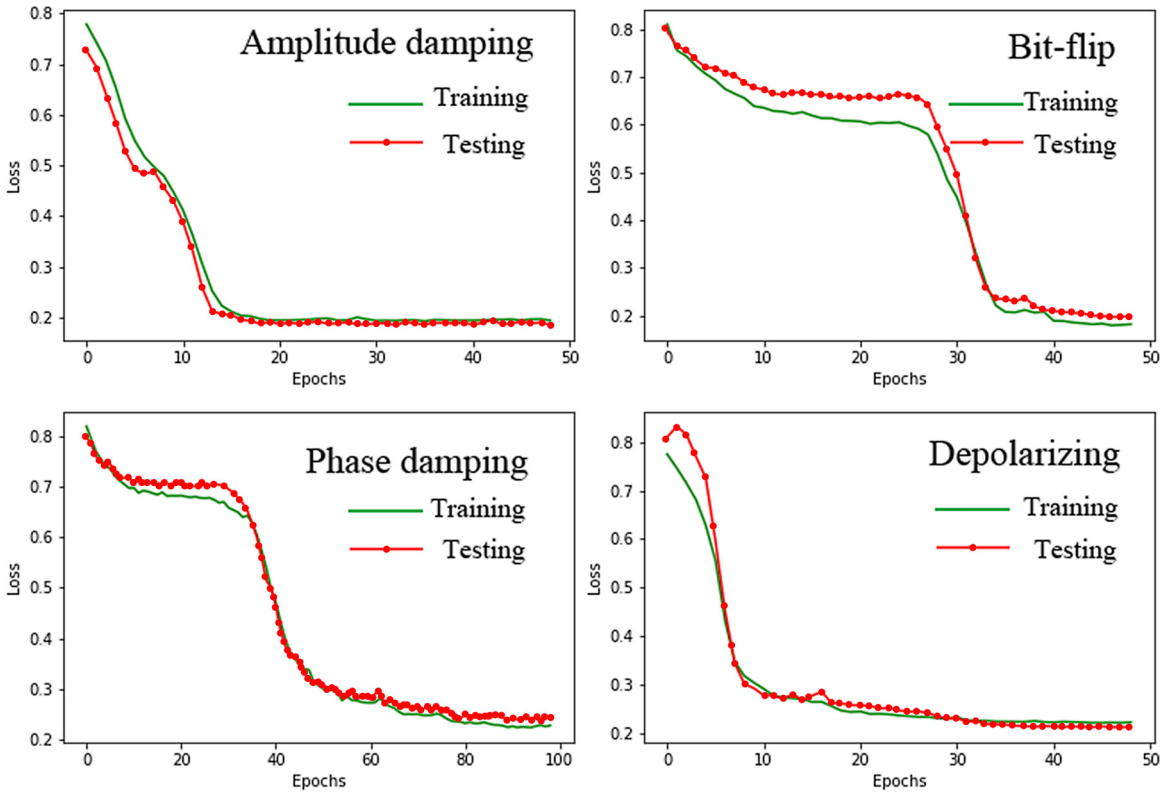

FIG. 9. Simulation results under the influence of amplitude damping noise, bit-flip noise, phase-flip noise and depolarizing noise.

them, the minimum value of fidelity of phase-flip noise and depolarizing noise reaches 0.80 and 0.71, respectively. It can be seen that the influence of different kinds of quantum noise on the quantum communication system cannot be ignored. Therefore, we superimpose the influence of different kinds of quantum noise on the system into the input quantum state of the quantum feedforward neural network of LAN receiver for training and testing and the corresponding loss functions are shown as Fig. 9

It can be observed from Fig. 9 that the loss function of the system finally converges to 0.18 after 12 epochs of training under the impact of amplitude damping noise and the loss function of testing data finally converges to 0.16. Relatively, after about 40 epochs of training, the loss function of the system under the influence of bit-flip noise converges to 0.16. The simulation result of testing data is not much different from the training data. For system under the influence of phase-flip noise, more than 60 epochs are required to stabilize the value of the loss function. Although the final value of loss function is not much lower than those of the first two noise, it is lower than 0.23. For system under the influence of depolarizing noise, the value of loss function drops dramatically in the first ten training epochs. At the end, the loss function of training data converges to 0.22 and the loss function of testing data converges to 0.21. In general, after dozens of epochs, the loss functions have fallen below 0.23, that is, the error rates are less than 0.23 under four kinds of quantum noise.

2. Mixed noise

(1) Amplitude damping and bit flip

Under the influence of amplitude damping noise and bit-flip noise, the fidelity of the system changes with the noise factors γ_{BF} and γ_{AD} as

$$F_{BF,AD}(|\beta_i\rangle, |c_i, \beta_i\rangle) = \begin{pmatrix} 0.16\gamma_{BF}\gamma_{AD} + 0.18\sqrt{1-\gamma_{AD}} \\ +0.64\gamma_{BF} - 0.08\gamma_{AD} + 0.18 \end{pmatrix}^{1/2}. \tag{26}$$

The corresponding curve of the function is shown as the first subgraph of Fig. 10. Under the influence of the superposition of two noise amplitude damping and bit flip, the fidelity of system decreases with the decrease of γ_{BF} and the increase of γ_{AD}. When $\gamma_{BF} = 0$, $\gamma_{AD} = 1$, the fidelity reaches the minimum value of 0.32.

The simulation result under the influence of amplitude damping noise and bit-flip noise is displayed through the change of the value of loss function with the increase of epochs in Fig. 11. In the first 11 epochs, the loss function dropped rapidly. In the end, the loss function of training data converges to 0.17 and the loss function of testing data converges to 0.16, that is, the error rate is less than 0.16.

(2) Amplitude damping and phase flip

Under the influence of amplitude damping noise and phase-flip noise, the fidelity of the system changes with the noise factors γ_{AD} and γ_{PF} as

$$F_{PF,AD}(|\beta_i\rangle, |c_i, \beta_i\rangle) = \begin{pmatrix} 0.36\gamma_{PF}\sqrt{1-\gamma_{AD}} + 0.08\gamma_{AD} \\ -0.18\sqrt{1-\gamma_{AD}} + 0.18 \end{pmatrix}^{1/2}. \tag{27}$$

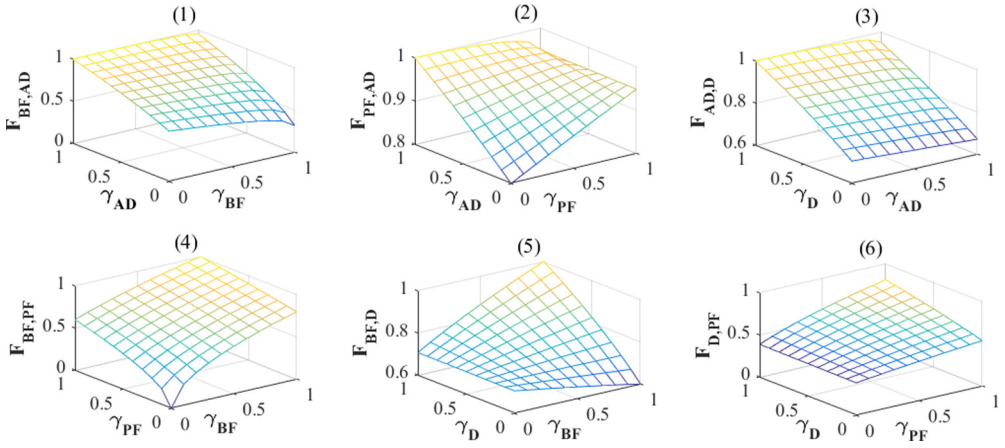

FIG. 10. The change of fidelity of the system with different combinations of noise factors γ_{AD}, γ_{BF}, γ_{PF}, and γ_D.

The corresponding curve of the function is shown as the second subgraph of Fig. 10. The fidelity of the system under the influence of amplitude damping noise and phase-flip noise reaches the minimum value of 0.8 when $\gamma_{PF} = \gamma_{AD} = 0$. At this time, the phase-flip noise is fully influenced on the system while the amplitude damping noise has no effect at all. When the two types of noise are completely superimposed on the system, the fidelity rises to 0.95. It means that, when phase-flip noise and amplitude damping noise act on the quantum system at the same time, the existence of amplitude damping noise will make the quantum state oscillate to a state closer to the original quantum state to a certain extent.

The simulation result under the influence of amplitude damping noise and phase-flip noise is displayed through the change of loss function with the increase of epochs in Fig. 12. In the first 37 epochs, the loss function decreases gradually. Finally, the loss function of training data converges to 0.23 and the loss function of testing data converges to 0.13, that is, the error rate is less than 0.13.

(3) Amplitude damping noise and depolarizing noise

Under the influence of amplitude damping noise and depolarizing noise, the fidelity of the system changes with the noise factors γ_{AD} and γ_D, as shown by

$$F_{D,AD}(|\beta\rangle, |c_i, \beta_i\rangle) = \begin{pmatrix} 0.13\gamma_D\gamma_{AD} + 0.18\sqrt{1-\gamma_{AD}}\gamma_D \\ -0.05\gamma_{AD} + 0.32\gamma_D + 0.5 \end{pmatrix}^{1/2}. \tag{28}$$

The corresponding curve of the function is shown as the third subgraph of Fig. 10. The system is not affected by noise when $\gamma_{AD} = 0$, $\gamma_D = 1$ and the fidelity is 1 at this time. With the increase of γ_{AD} and the decrease of γ_D, the fidelity of the system gradually decreases. When $\gamma_{AD} = 1$, $\gamma_D = 0$, the fidelity of the system decreases to the minimum value of 0.67. The second lowest point of the fidelity is about 0.7 when $\gamma_{AD} = \gamma_D = 0$ with only depolarizing noise acting on the quantum system.

The simulation result under the influence of amplitude damping noise and depolarizing noise is displayed through the change of the value of loss function with the increase of epochs in Fig. 13. In the first 10 epochs, the loss function decreases gradually. Finally, the loss functions of training and testing data converge to 0.20, that is, the error rate is less than 0.20.

(4) Phase flip and bit flip

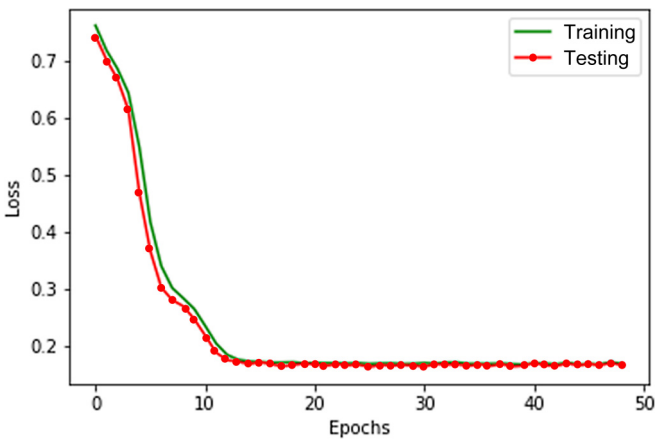

FIG. 11. Simulation result under the influence of amplitude damping noise and bit-flip noise.

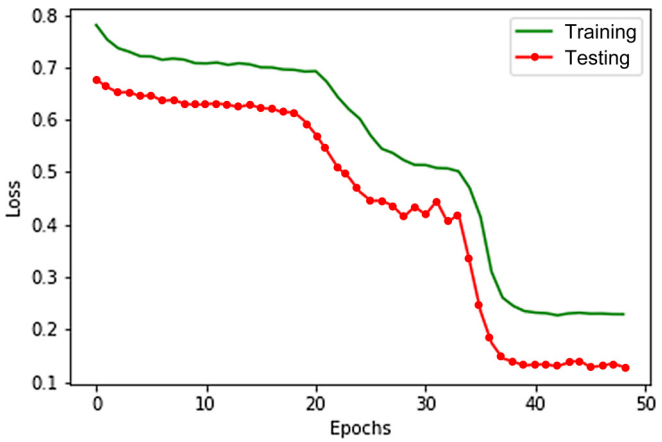

FIG. 12. Simulation result under the influence of amplitude damping noise and phase-flip noise.

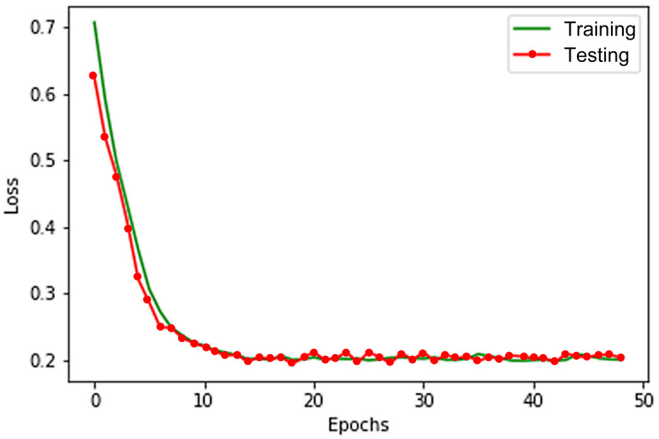

FIG. 13. Simulation result under the influence of amplitude damping noise and depolarizing noise.

Under the influence of phase-flip noise and bit-flip noise, the fidelity of the system changes with the noise factors γ_{PF} and γ_{BF}, as shown by

$$F_{PF,BF}(|\beta_i\rangle, |c_i, \beta_i\rangle) = (0.36\gamma_{PF} + 0.64\gamma_{BF})^{1/2}. \quad (29)$$

The corresponding curve of the function is shown as the fourth subgraph of Fig. 10. The system is not affected by noise when $\gamma_{PF} = \gamma_{BF} = 1$ and the fidelity is 1. The fidelity decreases gradually with the decrease of γ_{PF} and γ_{BF}. When the two noise are applied to the system completely with $\gamma_{PF} = \gamma_{BF} = 0$, the fidelity turns to zero. At the time only bit-flip noise acts on the system, the fidelity gradually decreases to 0.60 with the decrease of γ_{BF}. At the time only phase-flip noise acts on the system, the fidelity gradually decreases to 0.80 with the decrease of γ_{PF}.

The simulation result under the influence of phase-flip noise and bit-flip noise is displayed through the change of the value of loss function with the increase of epochs in Fig. 14. In the first 15 epochs, the value of loss function decreases gradually. Finally, the loss function of training data converges to 0.20 and the loss function of testing data converges to 0.18; that is, the error rate is less than 0.18.

(5) Depolarizing noise and bit-flip noise

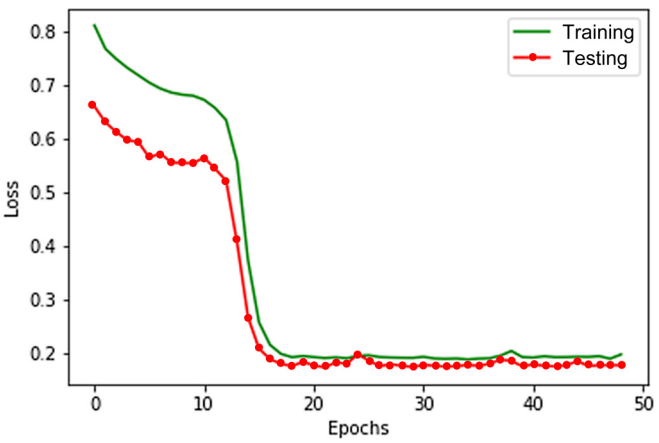

FIG. 14. Simulation result under the influence of phase-flip noise and bit-flip noise.

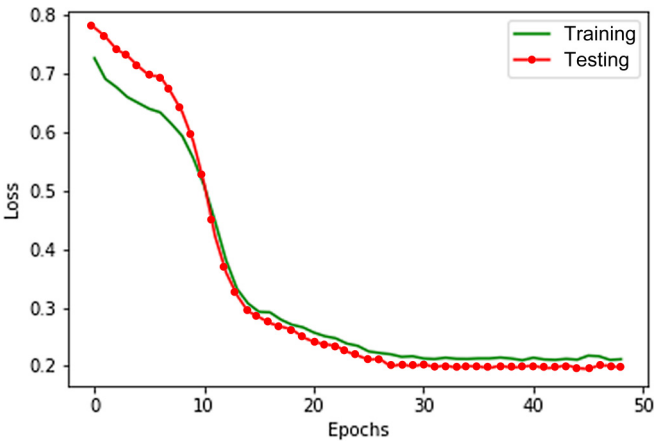

FIG. 15. Simulation result under the influence of depolarizing noise and bit-flip noise.

Under the influence of depolarizing noise and bit-flip noise, the fidelity changes with the noise factors γ_D and γ_{BF} as shown by

$$F_{D,BF}(|\beta_i\rangle, |c_i, \beta_i\rangle) = (0.36\gamma_D\gamma_{BF} + 0.14\gamma_D + 0.5)^{1/2}. \quad (30)$$

The corresponding curve of the function is shown as the fifth subgraph of Fig. 10. The system is not affected by noise when $\gamma_D = \gamma_{BF} = 1$ and the fidelity is 1. The fidelity decreases gradually with the decrease of γ_D and γ_{BF}. When the two noise are applied to the system completely with $\gamma_D = \gamma_{BF} = 0$, the fidelity turns to 0. 70. At the time only bit-flip noise acts on the system, the fidelity gradually decreases to 0.60 with the decrease of γ_{BF}. At the time only depolarizing noise acts on the system, the fidelity gradually decreases to 0.71 with the decrease of γ_D.

The simulation result under the influence of depolarizing noise and bit-flip noise is displayed through the change of the value of loss function with the increase of epochs in Fig. 15. In the first 13 epochs, the value of loss function decreases rapidly and decreased gradually in the next 17 epochs. Finally, the loss function of the training data converges to 0.20 and the

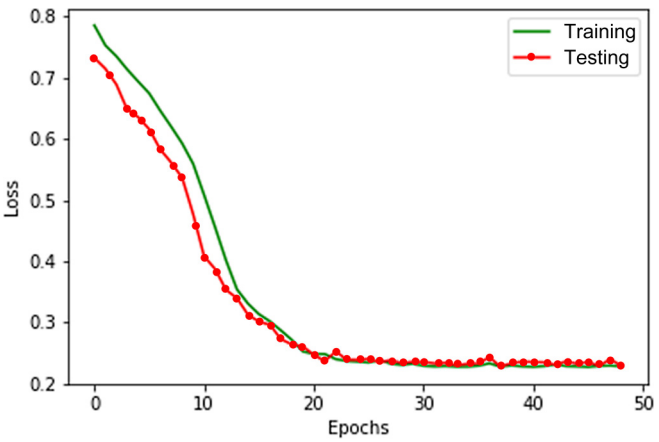

FIG. 16. Simulation result under the influence of depolarizing noise and phase-flip noise.

TABLE I. The error rates of LAN receiver under the influence of quantum channel noise.

Noise type	Single noise				Mixed noise					
	AD	BF	PF	D	AD & BF	AD & PF	AD & D	PF & BF	BF & D	PF & D
Error rate	0.18	0.16	0.23	0.21	0.16	0.13	0.20	0.18	0.18	0.21

loss function of the testing data converges to 0.18; that is, the error rate is less than 0.18.

(6) Depolarization noise and phase-flip noise

Under the influence of depolarizing noise and phase-flip noise, the fidelity changes with the noise factors γ_D and γ_{PF} as shown by

$$F_{D,PF}(|\beta_i\rangle, |c_i, \beta_i\rangle) = (0.36\gamma_D\gamma_{PF} + 0.14\gamma_D + 0.5)^{1/2}. \tag{31}$$

The corresponding change of the function is shown as the sixth subgraph of Fig. 10. The system is not affected by noise when $\gamma_D = \gamma_{PF} = 1$ and the fidelity is 1. The fidelity decreases gradually with the decrease of γ_D and γ_{PF}. When the two noise are applied to the system completely with $\gamma_{PF} = \gamma_{BF} = 0$, the fidelity turns to zero. 70. At the time only phase-flip noise acts on the system, and the gradually decreases to 0.70 with the decrease of γ_{PF}. At the time only depolarizing noise acts on the system, the fidelity gradually decreases to 0.80 with the decrease of γ_D. In this case, the depolarizing noise is more destructive to the system than the phase-flip noise.

The simulation result under the influence of depolarizing noise and bit-flip noise is displayed through the change of the value of loss function with the increase of epochs in Fig. 16. In the first 20 epochs, the value of loss function decreases rapidly. Finally, the loss function of the training and testing data converges to 0.20 in 50 epochs; that is, the error rate is less than 0.21.

C. Performance comparison

In Sec. IV B, we discussed the influence of quantum channel noise on the LAN receiver in detail. The error rate of the of LAN receiver is summarized in Table I. It can be obtained from simulation result shows that the maximum error rate is less than 0.23 and the minimum error rate is 0.13. The average error rate in all cases is 0.18.

The average error rate of LAN receiver is compared with various receivers: generalized Kennedy receivers including traditional Kennedy receivers and type-II receivers, CD Kennedy receivers and homodyne detection receivers in Table II. It can be seen from Table II that, when the average number N of thermal photons is greater than 0.85, the accuracy of LAN receiver proposed in this paper is higher than generalized Kennedy receivers and CD-Kennedy receiver. Compared with the homodyne receiver, the accuracy of LAN receiver is higher when the number of thermal photons is greater than 0.97.

V. CONCLUSION

To improve the antinoise performance and accuracy of optical quantum communication, an optimization strategy, learnable antinoise receiver inspired by quantum neural network is proposed in this paper. It is a universal optimization method that can be used in other communication protocols to improve antinoise ability and reduce communication error rate. In this optimization strategy, the displacement operator in the receiver is constructed by a quantum neural network which can update the parameters in the quantum circuit according to the noise affected training data until the combination of parameters with the lowest error rate is found. The experimental results show that the performance of LAN receiver under different kinds of strong noise is better compared with other type of receivers.

However, there are still some limitations of this work. First is the selection of alphabet. Since phase shift keyed alphabet has been applied widely in the relevant research, this paper chooses this type of alphabet to encode information for transmission. However, in some other cases, other alphabets like on-off keyed alphabet, may be more suitable. Due to the repeatability of content, we will supplement the related research in our future work. Second, in our numeral experiments, four kinds of common quantum channel noise and their different combinations are set as the turbulence. When it comes to simulation, we add the corresponding noise to the data set in advance. However, there still exists some difference between the simulated noise and the real one caused by the real quantum computers. If the experimental conditions get

TABLE II. Performance comparison of each receiver.

Receiver type	Variable value	Average error rate	Numerical trend of error rate compared with LAN receiver
Learnable antinoise receiver	None	$\leqslant$0.23	
Generalized Kennedy receiver	$N \leqslant 0.85$	$\leqslant$0.23	
	$N > 0.85$	$>$0.23	↑
CD-Kennedy receiver	$N \leqslant 0.85$	$\leqslant$0.23	
	$N > 0.85$	$>$0.23	↑
Homodyne receiver	$N \leqslant 0.97$	$\leqslant$0.23	
	$N > 0.97$	$>$0.23	↑

improved in the future, we expect to do our experiments on real quantum computers.

Overall, the optimized quantum communication algorithm and its physical implementation proposed in this paper has broad application in secure quantum communication, especially in the field of quantum key distribution. Since the large-scale commercial use of quantum communication is just around the corner, the coherent states, as the commonly used physical resource for quantum communication, will be transmitted through noisy quantum channels due to the situation that NISQ devices cannot provide noise-free environment for computation. Thus, our algorithm plays an important role in distinguishing quantum coherent states in the noisy environment for the implication of quantum communications.

In future research, we will pay more attention to improving the antinoise performance of the receivers and develop the receiver's ability to deal with more complex classification problems.

ACKNOWLEDGMENTS

This work was supported by Open Foundation of State Key Laboratory of Networking and Switching Technology (Beijing University of Posts and Telecommunications) (SKLNST-2020-1-17), PAPD and CICAEET funds.

[1] C. Silberhorn, T. C. Ralph, N. Lütkenhaus, and G. Leuchs, Continuous Variable Quantum Cryptography: Beating the 3 dB Loss Limit, Phys. Rev. Lett. **89**, 167901 (2002).

[2] A. M. Lance, T. Symul, V. Sharma, C. Weedbrook, T. C. Ralph, and P. K. Lam, No-Switching Quantum Key Distribution Using Broadband Modulated Coherent Light, Phys. Rev. Lett. **95**, 180503 (2005).

[3] H. X. Ma, P. Huang, W. S. Bao, and G. H. Zeng, Continuous-variable quantum identity authentication based on quantum teleportation, Quant. Info. Proc. **15**, 2605 (2016).

[4] Q. Li, Z. L. Li, W. H. Chan, S. Y. Zhang, and C. D. Liu, Blind quantum computation with identity authentication, Phys. Lett. A **382**, 938 (2018).

[5] F. G. Deng and G. L. Long, Secure direct communication with a quantum one-time pad, Phys. Rev. A **69**, 052319 (2004).

[6] C. Wang, F. G. Deng, Y. S. Li, X. S. Liu, and G. L. Long, Quantum secure direct communication with high-dimension quantum superdense coding, Phys. Rev. A **71**, 044305 (2005).

[7] J. Y. Hu, B. Yu, M. Y. Jing, L. T. Xiao, S. T. Jia, G. Q. Qin, and G. L. Long, Experimental quantum secure direct communication with single photons, Light: Sci. Appl. **5**, e16144 (2016).

[8] W. Zhang, D. S. Ding, Y. B. Sheng, L. Zhou, B. S. Shi, and G. C. Guo, Quantum Secure Direct Communication with Quantum Memory, Phys. Rev. Lett. **118**, 220501 (2017).

[9] R. Z. Yuan, M. F. Zhao, S. Han, and J. Cheng, Optimally displaced threshold detection for discriminating binary coherent states using imperfect devices, IEEE Trans. Comm. **69**, 2546 (2021).

[10] R. Z. Yuan and J. Cheng, Closed-form density matrices of free-space optical quantum communications in turbulent channels, IEEE Commun. Lett. **24**, 1072 (2020).

[11] R. Z. Yuan, M. F. Zhao, S. Han, and J. Cheng, Kennedy receiver using threshold detection and optimized displacement under thermal noise, IEEE Commun. Lett. **24**, 1313 (2020).

[12] M. F. Zhao, R. Z. Yuan, J. Cheng, and S. Han, Security of binary modulated continuous variable quantum key distribution using optimally displaced threshold detection, IEEE Commun. Lett. **25**, 1089 (2020).

[13] J. T. Kosloski, Ph.D. thesis, The Johns Hopkins University, 2012 (to to published).

[14] M. T. DiMario, L. Kunz, K. Banaszek, and F. E. Becerra, Optimized communication strategies with binary coherent states over phase noise channels, npj Quantum Inf. **5**, 65 (2019).

[15] M. Lassen, M. Sabuncu, A. Huck, J. Niset, G. Leuchs, N. J. Cerf, and U. L. Andersen, Quantum optical coherence can survive photon losses using a continuous-variable quantum erasure-correcting code, Nat. Photonics **4**, 700 (2010).

[16] M. Lassen, L. S. Madsen, M. Sabuncu, R. Filip, and U. L. Andersen, Experimental demonstration of squeezed-state quantum averaging, Phys. Rev. A **82**, 021801(R) (2010).

[17] M. Sabuncu, R. Filip, G. Leuchs, and U. L. Andersen, Environmental assisted quantum information correction for continuous variables, Phys. Rev. A **81**, 012325 (2010).

[18] M. Sabuncu, L. Mištra, Jr, J. Fiurášek, R. Filip, G. Leuchs, and U. L. Andersen, Nonunity gain minimal-disturbance measurement, Phys. Rev. A **76**, 032309 (2007).

[19] C. W. Helstrom, J. W. S. Liu, and J. P. Gordon, Quantum-mechanical communication theory, Proc. IEEE **58**, 1578 (1970).

[20] M. Takeoka and M. Sasaki, Discrimination of the binary coherent signal: Gaussian-operation limit and simple non-Gaussian near-optimal receivers, Phys. Rev. A **78**, 022320 (2008).

[21] R. L. Cook, P. J. Martin, and J. M. Geremia, Optical coherent state discrimination using a closed-loop quantum measurement, Nature (London) **446**, 774 (2007).

[22] F. E. Becerra, J. Fan, and A. Migdall, Photon number resolution enables quantum receiver for realistic coherent optical communications, Nat. Photonics **9**, 48 (2014).

[23] R. S. Kennedy, A near-optimum receiver for the binary coherent state quantum channel, Quart. Prog. Rep. **108**, 219 (1973).

[24] V. Vilnrotter and E. Rodemich, A generalization of the near-optimum binary coherent state receiver concept, IEEE Trans. Inf. Theory **30**, 446 (1984).

[25] R. S. Bondurant, Near-quantum optimum receivers for the phase-quadrature coherent-state channel, Opt. Lett. **18**, 1896 (1993).

[26] C. Wittmann, U. L. Andersen, and G. Leuchs, Discrimination of optical coherent states using a photon number resolving detector, J. Mod. Opt. **57**, 213 (2010).

[27] C. Wittmann, U. L. Andersen, M. Takeoka, D. Sych, and G. Leuchs, Demonstration of Coherent-State Discrimination Using a Displacement-Controlled Photon-Number-Resolving Detector, Phys. Rev. Lett. **104**, 100505 (2010).

[28] C. Wittmann, M. Takeoka, K. N. Cassemiro, M. Sasaki, G. Leuchs, and U. L. Andersen, Demonstration of Near-Optimal Discrimination of Optical Coherent States, Phys. Rev. Lett. **101**, 210501 (2008).

[29] R. P. Priya and A. Baradeswaran, An efficient simulation of quantum error correction codes, Alexandria Eng. J. **57**, 2167 (2018).

[30] L. T. Knoll, C. T. Schmiegelow, and M. A. Larotonda, Noisy quantum teleportation: An experimental study on the influence of local environments, Phys. Rev. A **90**, 042332 (2014).

[31] Z. G. Qu, S. Y. Wu, W. J. Liu, and X. J. Wang, Analysis and improvement of steganography protocol based on Bell states in noise environment, Comput. Mater. Contin. **59**, 607 (2019).

[32] R. Z. Yuan and J. Cheng, Free-space optical quantum communications in turbulent channels with receiver diversity, IEEE Trans. Comm. **68**, 5706 (2020).

[33] M. Schuld and N. Killoran, Quantum Machine Learning in Feature Hilbert Spaces, Phys. Rev. Lett. **122**, 040504 (2019).

[34] J. Wallnöfer, A. A. Melnikov, W. Dür, and H. J. Briegel, Machine learning for long-distance quantum communication, PRX Quantum **1**, 010301 (2020).

[35] Y. D. Cao, A. Daskin, S. Frankel, and S. Kais, Quantum circuit design for solving linear systems of equations, Mol. Phys. **110**, 1675 (2012).

[36] X. D. Cai, C. Weedbrook, Z. E. Su, M. C. Chen, M. Gu, M. J. Zhu, L. Li, N. L. Liu, C. Y. Lu, and J. W. Pan, Experimental Quantum Computing to Solve Systems of Linear Equations, Phys. Rev. Lett. **110**, 230501 (2013).

[37] P. Rebentrost, M. Mohseni, and S. Lloyd, Quantum Support Vector Machine for Big Data Classification, Phys. Rev. Lett. **113**, 130503 (2014).

[38] S. Lloyd, M. Mohseni, and P. Rebentrost, Quantum principal component analysis, Nat. Phys. **10**, 631 (2014).

[39] S. Lloyd and C. Weedbrook, Quantum Generative Adversarial Learning, Phys. Rev. Lett. **121**, 040502 (2018).

[40] I. Cong, S. Choi, and M. D. Lukin, Quantum convolutional neural networks, Nat. Phys. **15**, 1273 (2019).

[41] I. Kerenidis and A. Prakash, Quantum gradient descent for linear systems and least squares, Phys. Rev. A **101**, 022316 (2020).

[42] H. Kwon and J. Bae, A hybrid quantum-classical approach to mitigating measurement errors in quantum algorithms, IEEE Trans. Comput. **70**, 1401 (2021).

[43] P. Rebentrost, A. Steffens, I. Marvian, and S. Lloyd, Quantum singular value decomposition of non-sparse low-rank matrices, Phys. Rev. A **97**, 012327 (2018).